Mon. Not. R. Astron. Soc. **000**, 000–000 (0000) Printed 1 April 2015 (MN LATEX style file v2.2)

The role of 3-body H_2 formation in the fragmentation of primordial gas

Jayanta Dutta[1,2], Biman B. Nath[1], Paul C. Clark[2,3], Ralf S. Klessen[2]

[1] *Raman Research Institute, Sadashiva Nagar, Bangalore 560080, India*
[2] *Universität Heidelberg, Zentrum für Astronomie, Institut für Theoretische Astrophysik, Albert-Ueberle-Str. 2, 69120 Heidelberg, Germany*
[3] *School of Physics and Astronomy, Cardiff University, 5 The Parade, Cardiff CF24 3AA, UK*

1 April 2015

ABSTRACT

It has been shown that the behaviour of primordial gas collapsing in a dark matter minihalo can depend on the adopted choice of 3-body H_2 formation rate. The uncertainties in this rate span two orders of magnitude in the current literature, and so it remains a source of uncertainty in our knowledge of population III star formation. Here we investigate how the amount of fragmentation in primordial gas depends on the adopted 3-body rate. We present the results of calculations that follow the chemical and thermal evolution of primordial gas as it collapses in two dark matter minihalos. Our results on the effect of 3-body rate on the evolution until the first protostar forms agree well with previous studies. However, our modified version of GADGET-2 SPH also includes sink particles, which allows us to follow the initial evolution of the accretion disc that builds up on the centre of each halo, and capture the fragmentation in gas as well as its dependence on the adopted 3-body H_2 formation rate. We find that the fragmentation behaviour of the gas is only marginally effected by the choice of 3-body rate co-efficient, and that halo-to-halo differences are of equal importance in affecting the final mass distribution of stars.

Key words: stars: formation – stars: early universe – hydrodynamics – instabilities

1 INTRODUCTION

According to the standard model of the primordial star formation process, the very first stars, the so-called Population III (or Pop. III) stars form within dark matter (DM) halos with virial temperature ~ 1000 K and masses $\sim 10^6\ M_\odot$ that collapsed at redshift $z \sim$ 25-30 or above (Haiman et al. 1996; Tegmark et al. 1997; Abel et al. 2002; Glover 2005; Bromm & Larson 2004; Bromm et al. 2009). The hydrogen atoms in the DM halos combine with the small abundances of free electrons via $H + e^- \rightarrow H^- + \gamma$, followed by $H^- + H \rightarrow H_2 + e^-$, where the free electrons act as catalysts and are present as residue from the epoch of recombination at $z \sim 1100$ (Barkana & Loeb 2001; Ciardi & Ferrara 2005).

The typical fractional abundances of H_2 of $\sim 10^{-3}$ are sufficient to permit the primordial gas in the minihalos to cool as it collapses (see, e.g. Susa et al. 1998; Yoshida et al. 2003) via H_2 rotational and vibrational line emission. This occurs until the gas reaches a temperature $\sim$ 200K (Omukai & Nishi 1998) at a density of $\sim 10^4 \mathrm{cm}^{-3}$, at which point the H_2 energy levels move into the local thermodynamical equilibrium (LTE) with the kinetic temperature of the gas, and the resulting cooling time becomes longer than the free-fall of the gas. The gas now heats up slightly as the collapse proceeds. This transition from cooling to heating with increasing density sets a characteristic Jeans length, allowing the gas to fragment with Jeans mass of $M_\mathrm{J} \sim 1000 M_\odot$ at typical temperatures of $T \sim 200\,\mathrm{K}$ and number densities $n \sim 10^4\,\mathrm{cm}^{-3}$ (Abel et al. 1998, 2002; Bromm et al. 1999, 2002).

Once the gas reaches a number density of $\sim 10^8 \mathrm{cm}^{-3}$, further H_2 formation is possible via the 3-body reactions (Palla et al. 1983):

$$H + H + H \rightarrow H_2 + H \quad (1)$$

$$H + H + H_2 \rightarrow H_2 + H_2. \quad (2)$$

Unfortunately, the rate coefficients for the above set of reactions are very uncertain in the temperature regime which

is applicable to Pop. III star formation, with the current estimates in the literature spanning two orders of magnitude (see Glover & Abel 2008; Glover & Savin 2009 for discussion). However, independent of the choice of rate coefficient, calculations of the gravitational collapse of primordial gas show that by a number density of $\sim 10^8 \mathrm{cm}^{-3}$, almost all the atomic hydrogen is converted to H_2 (Yoshida et al. 2006; Turk et al. 2009).

The sudden formation of H_2 has two interesting effects. First, the process is accompanied by heating, since 4.4 eV is released for every H_2 molecule that is formed. If the formation rate is fast enough, this heating can momentarily stall the collapse against collapse. On the other hand, the ability of the gas to cool is proportional to (among other things) the fractional abundance of H_2, so the more H_2 is formed, the more the gas can cool. In practise, the interplay between these two phenomena is complex, and depends crucially on the adopted rates for the 3-body reactions (Turk et al. 2011). Under certain conditions, a chemo-thermal instability can also occur that may promote the gas to fragment (Yoshida et al. 2007; Greif et al. 2013).

In addition to any fragmentation induced by the chemo-thermal instability, recent simulations conclude that the disk around the first primordial protostar becomes gravitationally unstable and forms a multiple system with low-mass protostars instead of a single protostar (Clark et al. 2008, 2011b; Stacy et al. 2010; Greif et al. 2011; Smith et al. 2011; Dopcke et al. 2013). This can occur on timescales as short as 10 to 100 years after the formation of the first object. Clark et al. (2011b) show that the fragmentation of this disc results from the fact that the disc is unable to accrete onto the protostar faster than it accretes from the in-falling envelope.

The study by Turk et al. (2011) used both SPH and AMR simulations to conclude that the choice of 3-body-rate coefficients can introduce significant uncertainty into the radial velocity, temperature and accretion rate, and therefore can affect the rate at which the protostellar disc is fed. This has recently been verified by Bovino et al. (2014), who used both old rates and newly calculated improved rate given by Forrey (2013), to reach similar conclusion as Turk et al. (2011). Although they found compressed spiral arms, with strong density contrast between the arms and embedding medium, these simulations were unable to follow the evolution beyond the formation of the protostar, and so could not address the long-term behaviour of the disc structure.

However the degree to which the disc fragmentation depends on the chemical uncertainties in the 3-body H_2 formation rate has never been systematically tested. Previous studies did not include sink particles, and could not study the fragmentation that occurs once the first object is formed. In this work we focus on the effect that the choice of 3-body reaction rate has on the fragmentation of the primordial gas.

2 NUMERICAL METHODOLOGY

2.1 Simulation setup

We investigate two minihaloshalos obtained from the cosmological simulations of Greif et al. (2011, 2012), which used the hydrodynamic moving mesh code *Arepo* (Springel 2010). We use the snapshots from these simulations at a point when the central number density is just below 10^6 cm^{-3} – comfortably before the onset of the 3-body reactions – as the starting point for this project. Interpreting the mesh-generating points of *Arepo* as Lagrangian fluids particles, we then use the *Arepo* output as the initial conditions for our GADGET-2 (Springel 2005) implementation. The modifications to the standard GADGET-2 include a time-dependent chemical network for primordial gas, and a sink particles to capture the formation of collapsing protostellar cores (Bate et al. 1995; Jappsen et al. 2005). A fuller description of the code and its features can be found in Clark et al. (2011a,b). The conversion from the moving mesh to smoothed-particle hydrodynamics (SPH) formalism is the same as that performed by Smith et al. (2011), and indeed the minihalos are identical, both in terms of the baryonic and dark matter content.

The original *Arepo* simulations resolve the Jeans length with 128 cells (Greif et al. 2011), at which point further refinement is deactivated, resulting in roughly constant mass particles within central $\approx$ 1000 AU. However, to investigate the effect of 3-body H_2 reactions, here we use the intermediate *Arepo* snapshots (when the central number density $n \leqslant 10^6$ cm^{-3}) as the starting point. Although the initial size of the minihalos are ≈ 3 pc, all the fragmentation and accretion take place in the central region of the halos where the SPH particle masses are roughly 10^{-4} $M_\odot$. In GADGET-2 simulation the mass resolution for 100 SPH particles (e.g. Bate & Burkert 1997) is $\approx 10^{-2}$ $M_\odot$.

The chemical and thermodynamical treatment of the gas in the *Arepo* simulations of Greif et al. (2011) is also identical to those in our GADGET-2 implementation for the range of densities that are studied in this paper. More details of the initial conditions for this study are given below.

Of the various rates available in the literature for the 3-body H_2 formation reactions, we choose the extreme rate coefficients: the slowest of which is Abel et al. (2002) (hereafter ABN02) alongside that of Flower & Harris (2007) which provides the fastest of the rates (hereafter FH07). We have used the collisional-dissociation rate in the LTE limit as described in Turk et al. (2011). For our SPH calculation we used a temperature-dependent value calculated via the principle of detailed balanced. For the ABN02 runs, data from Orel (1987) are used for low density (and low temperature, $T < 300$ K) cases, and a power law (described in Table 1) for high density and temperatures. For FH07 runs, we used the rates given in Flower & Harris (2007). For the radiative cooling rate, we use Sobolev approximation to calculate it in the optically thick region, as described in detail in Clark et al. (2011a) and Yoshida et al. (2006). Full details of these rates are given in Table 1.

Ref	3-body H_2 formation rates, k_{3bh2} ($cm^6\ s^{-1}$)	Temp range
ABN02	$1.3 \times 10^{-32}(T/300)^{-0.38}$	$(T < 300K)$
ABN02	$1.3 \times 10^{-32}(T/300)^{-1.00}$	$(T > 300K)$
FH07	$1.44 \times 10^{-26}/T^{1.54}$	
H_2 collisional dissociation rates ($cm^3\ s^{-1}$)		
ABN02	$\frac{1.0670825\times10^{-10}\times(T/11605)^{2.012}}{\exp(4.463/T/11605)\times(1+0.2472\ T/11605)^{3.512}}$	
FH07	$1.38 \times 10^{-4} \times T^{-1.025} \exp(-52000/T)$	

Table 1. Summary of 3-body H_2 formation and dissociation rates adopted here.

2.2 Initial Conditions

The simulations with halo1 start with a maximum central cloud number density (n) $10^6 cm^{-3}$ and minimum n of $71 cm^{-3}$. The initial temperature of the atomic hydrogen is 470K (max) and 60K (min). Halo1 contains $1030 M_\odot$ of gas and 690855 SPH particles. The maximum and minimum mass of SPH particles are 0.16 $M_\odot$ and 1.3 $\times 10^{-4}$ $M_\odot$. This means that the numerical resolution of our simulations for halo1 for 100 SPH particles is 1.3 $\times 10^{-2}$ $M_\odot$. The simulations with halo2 starts with a maximum n of $10^6 cm^{-3}$ and minimum n of $85 cm^{-3}$. The initial temperature of the atomic hydrogen is 436K (max) and 54K (min). Halo2 contains $1093 M_\odot$ of gas and 628773 SPH particles. The maximum and minimum mass of SPH particles are $0.05 M_\odot$ and 1.4 $\times 10^{-4}$ $M_\odot$. This means that the numerical resolution of our simulations for halo2 for 100 SPH particles is 1.4 $\times 10^{-2}$ $M_\odot$. With altogether 6 million particles in the simulation, we resolve the halo gas and its velocity structure significantly better than in the SPH models of our previous study (Turk et al. 2011). However, we note that none of the existing numerical calculations are able to fully resolve the turbulent cascade in the halo gas and do justice to the large Reynolds numbers (of 10^9 or above) that characterise the accretion flow (see, e.g. chapter 4 in Klessen & Glover 2015).

Each of the minihalos are simulated with the two contrasting 3-body reaction rates, resulting in 4 simulations in total. The different minihalos allow us to distinguish between those features of the high-density collapse/evolution that are caused by the chemo-thermal differences arising from the reaction rates, and those features which result from cosmic variance (i.e. differences caused by the formation of the minihalos).

As collapse progresses in the central region of the cloud, sink particles are created once the number density of the gas reaches 5 $\times 10^{13} cm^{-3}$, at which point the gas has a temperature of around 1000K. The corresponding Jeans mass at this density and temperature is $0.06 M_\odot$, so our calculations for both of the halos are well resolved. We replace a candidate particle by a sink particle (see, e.g. Bate et al. 1995; Krumholz et al. 2004; Jappsen et al. 2005) that can accrete gas particles within its accretion radius r_{acc} that we fix at 6 AU, which is the Jeans radius at the density threshold for sink creation. We also prevent sink particles from forming within $2\,r_{acc}$ of one another in order to avoid spurious formation of new sink particles out of gas that, in reality, would by accreted by a neighbouring sink particle. Lastly, gravitational interactions between sinks, and between the sinks and the gas, are softened using a fixed softening parameter of 1.2 AU for the sinks. We run our simulations until a mass of 21 $M_\odot$ has been accreted by all the sink particles.The final time scales range between 2500–4000 yr due to the physical differences between the minihalos and the 3-body H_2 formation rates.

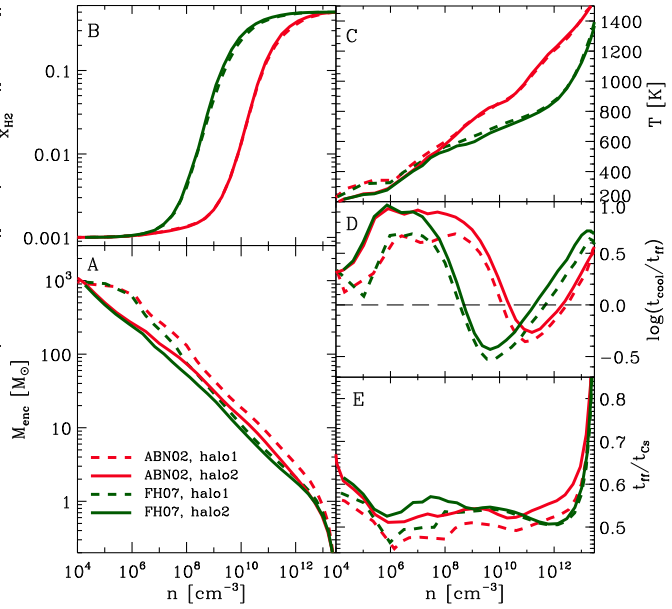

Figure 1. Radially binned, mass-weighted averages of physical quantities for different 3-body H_2 formation rate (red: ABN02, green: FH07) of two different cosmological halos (dotted: halo1, solid: halo2), are compared just before the first protostar forms. The enclosed mass (A), H_2 fraction (B), temperature (C), ratio of cooling time to free-fall time (D) and ratio of free-fall time to sound-crossing time (E) are plotted as a function of number density.

3 PHYSICAL CONDITIONS JUST BEFORE SINK PARTICLE CREATION

In this section we examine the physical conditions in the gas once the central region has collapsed to a density of $\sim 5 \times 10^{13}$ cm^{-3}. The radial profiles of the gas for the two different halos and two different 3-body rates are shown in Figure 1. The panels show mass-weighted averages of the properties of individual SPH particles within radial logarithmic bins.

Panel A shows the mass enclosed as a function of the number density, and we see that it displays a rough power-law over most of the density range covered here. This simply follows from the radial power-law in the density which is typical for primordial gas: $n(r) \propto r^{-2.2}$ (e.g. Abel et al. 2002;

Yoshida et al. 2006, 2008). We see that there are slight differences between the profiles for the two rates, but these are also comparable to the differences between the two halos.

In panel B, we see the rapid rise in the H_2 fraction with increasing density that arises from the 3-body reactions. Here we see a clear difference between the two rates, with the runs with FH07 producing most of the H_2 by a density of 10^9 cm^{-3}, while the ABN02 runs are only starting to produce H_2 by the time this density is reached. As the rates are a strong function of density, we see very little difference in the H_2 fractions between the two halos.

The mean temperature as a function of the number density is shown in panel C. We find that the gas is significantly cooler, up to a factor of 2, around density $\sim 10^{12}$ cm^{-3}, in the FH07 halos than in those using ABN02. The differences in temperature-density evolution start around a number density of 10^7 cm^{-3}, once the H_2 abundance in the FH07 case has increased by an order of magnitude. Again, we find that there is little difference between evolution of halos 1 and 2 in this panel, implying that the chemical state of the gas is more important for the temperature evolution than any differences in the halo properties. Curves in panels A, B and C are consistent with the results of Turk et al. (2011).

4 VELOCITY STRUCTURE AND ACCRETION

In this section we study the difference in mass accretion associated with the cloud collapse, that can arise due to the choice of 3-body reaction rates. In what follows, we will first study the accretion rate as predicted by the properties of the gas in the clouds just before the first sink particle forms. We will then examine the accretion rate as measured by the sink particles themselves.

The accretion rate can be estimated from the radial gas profiles using,

$$\dot{M}(r) = 4\,\pi\,r^2\,\rho(r)\,v_{\rm rad}(r). \quad (3)$$

This has been shown to be a good estimate of the accretion rate (Clark et al. 2011a). In addition, one can define an accretion time from,

$$t_{\rm acc} = \frac{M_{\rm enc}(r)}{4\,\pi\,\rho\,v_{\rm rad}\,r^2}. \quad (4)$$

Since accretion is related to infall velocity, we also discuss the corresponding radial and rotational velocities. Figure 2 shows these physical quantities as the function of enclosed mass for all the simulations, using the radial profiles in the gas just before the formation of the first sink particle. The left panel of Figure 2 in the clockwise order, shows the accretion rate, radial velocity, radial velocity over sound speed and accretion time respectively. Similarly the right panel of Figure 2 shows the rotational velocity, radial velocity over rotational velocity, rotational velocity over Keplerian velocity and rotational velocity over sound speed respectively in the clockwise order.

We note that the mass accretion rate ($\dot{M}$) for all the simulations has a maximum at an enclosed mass $\sim$ 1–2 $M_\odot$. Given that H_2 line-cooling becomes optically thick at the corresponding densities for this enclosed mass, it makes sense that $\dot{M}$ for all the simulations converge at this mass scale, as the gas loses its ability to cool efficiently. In general the differences in accretion rates caused by the choice of 3-body formation rate are small, around 25 percent. The differences between the rates in different halos are much larger, at around a factor of 2 for masses below a few tens of solar mass. However we see from the top left panel of Figure 2 that once the mass approaches 100 $M_\odot$, the difference in the accretion rates can be large, approaching an order of magnitude. We conclude that halo-to-halo variations will play a larger role in the accretion rates than chemical uncertainties.

The choice of 3-body rate coefficient introduces difference in radial velocity of $\sim$ 0.4–0.5 km s^{-1}. We also note that the radial velocities for both rates are substantially lower than the rotational velocities. The gas particles spiral inwards with trajectories following a combination of gravitational attraction and angular momentum conservation. All clouds are sub-Keplerian. However, there is a slight tendency for the gas to be more rotationally supported in the FH07 runs – at least for the inner 10 $M_\odot$ of gas.

We can compare these results with both the AMR and SPH simulations of Turk et al. (2011). Our high-resolution study also concludes that the difference in the 3-body H_2 formation rates significantly affect the dynamical behaviour of the collapsing gas. The uncertainty in the velocity structure has also been investigated by Bovino et al. (2014) using hydrodynamics code ENZO. They also found that there are relatively large differences in the radial velocities of about 2–3 km s^{-1} depending on the halo distribution as well as 3-body H_2 formation rates.

Although there is scatter in the velocities for ABN02 and FH07 rates, the scatter also exists in the velocities for both halo1 and halo2. We again conclude that the halo-to-halo differences in the velocity structure is, in general, more pronounced than that caused by the differences in the chemical reaction rates.

5 FRAGMENTATION

We have shown in Section 2.2 that the temperature of the gas at high densities, such as those in disc, depends on the choice of adopted 3-body H_2 formation rate. In this section, we study how the gas fragments as it evolves beyond the formation of the first collapsing core. Our discussion will first focus on the properties of the gas, to see whether there is any hint of the future evolution already present before the first sink particle forms. We will then compare the properties of the sink particles in the simulations and discuss the differences.

One useful measure of the ability of the gas to fragment is the ratio of the thermal to gravitational energy. This can be represented by the number of Bonnor-Ebert masses ($M_{\rm BE}$) contained in the central dense volume (Ebert 1955; Bonnor 1956). We therefore investigate the changes in the number (i.e, $M_{\rm enc}/M_{\rm BE}$) for each of our simulations and how it varies

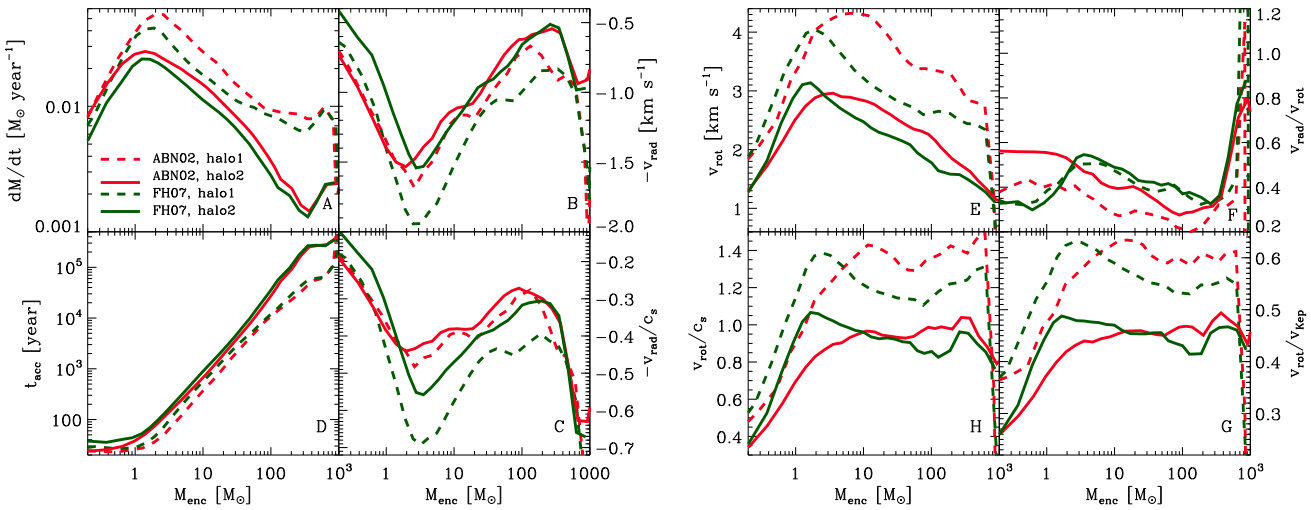

Figure 2. Radial logarithmic binned, mass-weighted averages of mass accretion rate (A), radial velocities (B), ratio of radial velocity to sound speed (C), accretion time (D), rotational velocity (E), ratio of radial to rotational velocity (F), ratio of rotational to Keplerian velocity (G), and ratio rotational velocity to sound speed (H) are plotted as a function of enclosed mass. The halo to halo variation as well as the uncertainty in the 3-body rate introduce an uncertainty in the mass accretion rate, radial and rotational velocity.

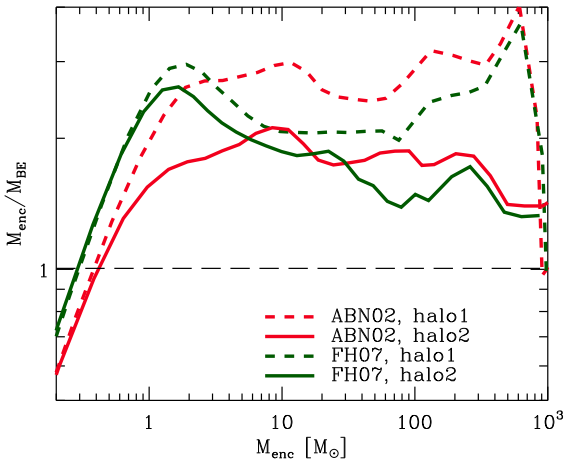

Figure 3. The number of Bonnor-Ebert masses ($M_{\rm enc}/M_{\rm BE}$) in the central dense volume is plotted as a function of enclosed mass, just before formation of first protostar. The degree of gravitational instability for FH07 within the central dense regime is larger than ABN02, indicating larger opportunity for the gas to fragment in the FH07 case, than in the ABN02 simulations.

with the enclosed gas mass, similar to the analysis performed by Abel et al. (2002). We computed the Bonnor-Ebert mass as the mass-weighted average within the logarithmic radial bin,

$$M_{\rm BE} = 1.18(c_s^4/G^{3/2})P_{\rm ext}^{-1/2} \approx 20 M_\odot T^{3/2} n^{-1/2} \mu^{-2} \gamma^2, \qquad (5)$$

where c_s is the sound speed, $P_{\rm ext}$ is the external pressure that we assume to be equal to the local gas pressure, μ is the mean molecular weight and $\gamma = 5/3$ is the adiabatic index respectively.

The results are shown in Fig. 3. Note that the ratio $M_{\rm enc}/M_{\rm BE}$ is equivalent to the ratio of fragmentation timescale to that of accretion, $t_{\rm frag}/t_{\rm acc}$. Once again, these snapshots were taken immediately before the formation of the first protostar. The dashed lines represent the case when fragmentation timescale equals the accretion timescale.

While we see that there are differences between the mass profiles of the FH07 and ABN02 runs, the effects are, once again, not substantial. However, in the case of $M_{\rm enc}/M_{\rm BE}$ we see that the FH07 runs have a differently shaped profile from the ABN02 runs (top panel of Fig. 3). In the FH07 case, the profiles are peaked at characteristic mass of 1-2 $M_\odot$. In contrast, the ABN02 runs do not display such a peak, and it is less clear whether these runs would favour a particular mass for fragmentation.

If the ratio $M_{\rm enc}/M_{\rm BE} < 1$ the gas enclosed in the shells are accreted faster than it can fragment. As a result fewer new protostars are formed and the available mass contributes to the mass growth of the existing ones (Dopcke et al. 2013). In our case we find $M_{\rm enc}/M_{\rm BE} > 1$, i.e., the gas in the shells can fragment faster than it is accreted by the central dense clump, favouring low-mass protostars.

Therefore by considering the radial density profiles before the onset of sink formation we conclude that gas in FH07 case is perhaps more likely to fragment than in the ABN02 case. Next we study how the gas fragments at later epochs after formation of the first sink particle. We follow the simulations until 21 $M_\odot$ have been converted into, or accreted onto, sink particles.

We have calculated the total mass accretion rate by all the sinks particles. Although fragmentation may depend

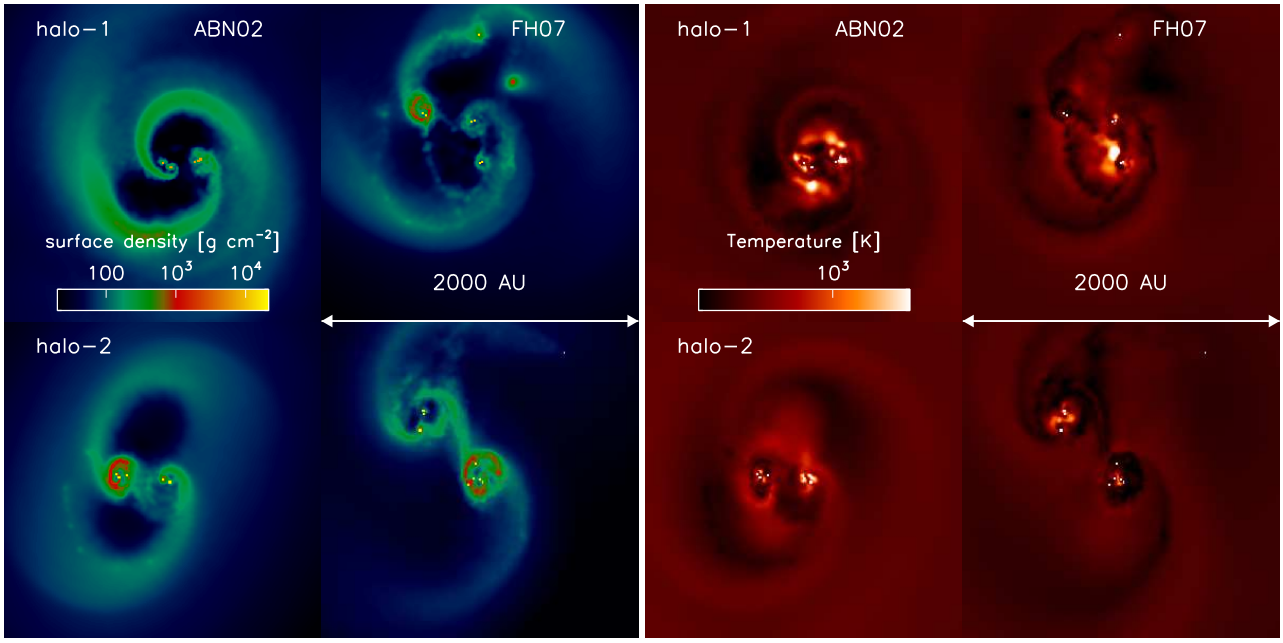

Figure 4. Surface density and temperature in a region of 2000 AU centred around first protostar for different 3-body H_2 formation rates, are shown when the total mass of the sinks reaches $\sim 21\,M_\odot$.

on the way sink particles are modelled, our implementation (Section 2.2) takes considerable care to avoid what is often called artificial fragmentation and the spurious formation of sink particles (further details are found in Clark et al. 2011b, see also Bate et al. 1995, Jappsen et al. 2005, and Federrath et al. 2010).

The column density and column-weighted temperature distribution in the inner 2000 AU at the end of the simulations are shown in Figure 4. In all cases we see that the simulations exhibit disc structure on several scales within this central region. It is not surprising, given the high levels of rotational support seen in right-hand panel in Figure 2. We also see that the temperatures in the disc are slightly less in the case with the FH07 rate, due to the increased H_2 fraction. However from these images it is clear that all simulations fragment to form a small-N system within the time that $21\,M_\odot$ of material is accreted onto sink particles.

Figure 5A shows the time evolution of total mass accretion rate onto the sinks (same as Figure 2). The plot shows that mass accretion rate for ABN02 is larger than the FH07 rate. For both rates, dM_*/dt decreases with time. After ≈ 500 years, further sink particles form, and the total accretion rate increases again, however, now with large temporal variations. In Figure 5B, we plot the mass accretion rate as a function of total sink mass. Figure 5C shows the time evolution of the total mass in sinks and Figure 5D shows the maximum sink mass in the period over which the sink formation occurs.

We see that the simulations employing the ABN02 rate produce a maximum sink mass that is consistently above the FH07 rate, for a given halo. However, the difference is less than a factor of 2 and is similar to the inter-halo difference. When we examine Figure 5E, which shows the total number of sink particle versus the total mass in all sinks, we see a similar behaviour: the differences between the runs with different rates can be a factor of two. Although in this case the halo-to-halo differences are less pronounced.

We caution the reader that our simulations do not include feedback effects from nascent protostars. We therefore restrain ourselves from following the dynamical evolution of the embedded stellar system over very long timescales. We end our calculations before we expect that radiative and mechanical feedback changes the thermal as well as chemical state – and as a consequence – also modifies the fragmentation behavior of the remaining gas (see, e.g., the discussion in Wise & Abel 2008, Whalen et al. 2010, Hosokawa et al. 2011, or Stacy et al. 2012).

6 SUMMARY

We have investigated the effects of different proposed 3-body H_2 formation rates during the collapse of primordial star-forming clouds and analysed their influence on the resulting fragmentation behaviour of the gas. We compared the rates proposed by Abel et al. (2002) and by Flower & Harris (2007), which span two orders of magnitude. We follow the chemical and thermal evolution of the primordial gas in two different minihalos in order to assess differences introduced by varying halo parameters. We find that the uncertainty in the 3-body H_2 formation rates leads to the differences in the chemical state of the gas which is more important for the thermal evolution of the clouds than any differences in the

halo properties. The halo to halo variation affects the dynamical evolution of the gas and mass-accretion more than the chemical uncertainties.

We also find that the simulations employing the Abel et al. (2002) rate to produce on average fewer and more massive fragments compared to those calculations using the Flower & Harris (2007) rate (consistent with the results of Bovino et al. (2014) which however did not use sink particles). This difference of roughly a factor of two, however, is comparable to the halo-to-halo variation. This is similar to the results reported by Turk et al. (2011) with added advantage of using sink particles.

In summary, we find that the variations introduced to the mass distribution of primordial stars introduced by the uncertainties in the three-body H_2 formation rate is of similar order to the fluctuations introduced by difference in the halo properties.

The authors wish to thank Thomas Greif for providing the data of the minihalos on which our analysis is based. The authors also acknowledge Simon Glover, Andrea Ferrara, Kazukai Omukai, Mahavir Sharma for helpful comments. J.D. is grateful to the Raman Research Institute for financial support and hospitality. All the computations described here were performed on the HPC-GPU Cluster Kolob (funded by Heidelberg University and Deutsche Forschungsgemeinschaft). RSK acknowledges support from the European Research Council under the European Community's Seventh Framework Programme (FP7/2007-2013) via the ERC Advanced Grant 'STARLIGHT: Formation of the First Stars' (project number 339177).

REFERENCES

Abel, T., Anninos P., Norman, M. L., Zhang Y., 1998, ApJ, 508, 518
Abel, T., Bryan, G. L., & Norman, M. L. 2002, Science, 295, 93
Bate, M. R., Bonnell, I. A., Price, N. M. 1995, MNRAS, 277, 362
Barkana, R., Loeb, A., 2001, Phys. Rep., 349, 125
Bate, M. R., Bonnell, I. A. & Price, N. M. 1995, MNRAS, 277, 362
Bate, M. R., Burkert, A., 1997, MNRAS, 288, 1060 B
Bovino, S., Schleicher, D. R. G., Grassi, T., 2014, A&A, 561A, 13B
Bromm, V., Coppi, P. S., & Larson, R. B., 1999, ApJ, 527L, 5B
Bromm, V., Coppi, P. S., & Larson, R. B., 2002, ApJ, 564, 23
Bromm, V., & Larson, R. B. 2004, ARA&A, 42, 79
Bromm, V., Yoshida, N., Hernquist, L. & McKee, C. F. 2009, Nature, 459, 49
Bonnor, W., B. 1956, MNRAS, 116, 351
Ebert, R., Z. 1955, Astrophys, 37, 217
Ciardi, B. & Ferrara A, 2005, Space Sci. Rev., 116, 625
Clark, P. C., Glover, S. C. O., & Klessen, R. S. 2008, ApJ, 672, 757
Clark, P. C., Glover, S. C. O., Klessen, R. S. & Bromm, V. 2011a, ApJ 727 110
Clark, P. C., Glover, S. C. O., Smith, R. J., Greif, T. H., Klessen, R. S. & Bromm, V. 2011b, Science, 331, 1040
Dopcke, G; Glover, S C. O.; Clark, P. C.; Klessen, R. S., 2013, ApJ, 766, 103D
Federrath, C.; Banerjee, R.; Clark, P. C.; Klessen, R. S., 2010, ApJ, 713, 269
Flower, D. R., & Harris, G. J. 2007, MNRAS, 377, 705
Forrey, R. C., 2013, ApJ, 773L, 25F
Glover, S. 2005, Space Sci. Rev., 117, 445
Glover, S. C. O., & Abel, T. 2008, MNRAS, 388, 1627
Glover, S. C. O. & Savin, D. W., 2009, MNRAS, 393, 911
Greif, T. H.; Springel, V.; White, S. D. M.; Glover, S. C. O.; Clark, P. C.; Smith, R. J.; Klessen, R. S.; Bromm, V., 2011, ApJ, 737, 75G
Greif, T. H.; Bromm, V; Clark, P. C.; Glover, S. C. O.; Smith, R. J.; Klessen, R. S.; Yoshida, N.; Springel, V, 2012, MNRAS, 424, 399G
Greif, T. H.; Springel, V.; Bromm, V, 2013, MNRAS, 434, 3408G
Haiman, Z.; Thoul, A. A.; Loeb, A, 1996, ApJ, 464, 523H
Hosokawa, T., Omukai, K., Yoshida Naoki & Yorke H. W. 2011, Science, 334, 1250
Jappsen, A.-K., Klessen, R. S., Larson, R. B., Li, Y., & Mac Low, M.-M. 2005, A&A, 435, 611
Klessen, R. S., Glover, S. C. O., lecture notes of the 43rd Saas Fee Advanced Course *Star Formation in Galaxy Evolution: Connecting Numerical Models to Reality*, ed. Y. Revaz (Springer Publishing), arXiv:1412.5182
Krumholz, M. R., McKee, C. F. & Klein, R. I., 2004, ApJ, 611, 399
Omukai, K., & Nishi, R. 1998, ApJ, 508, 141
Omukai, K., Tsuribe, T., Schneider, R., & Ferrara, A. 2005, ApJ, 626, 627
Orel, A. E., 1987, J. Chem. Phys., 87, 314
Palla, F., Salpeter, E. E., & Stahler, S. W. 1983, ApJ, 271, 632
Smith, R. J.; Glover, S. C. O.; Clark, P. C.; Greif, T.; Klessen, R. S., 2011, MNRAS, 414, 3633S
Stacy, A., Greif, T. H., & Bromm, V., 2012, MNRAS, 422, 290S
Susa, H.; Uehara, H.; Nishi, R.; Yamada, M., 1998, PThPh, 100, 63S
Springel, V., 2005, MNRAS, 364, 1105
Springel, V., 2010, MNRAS, 401, 791S
Stacy, A., Greif, T. H., & Bromm, V. 2010, MNRAS, 403, 45
Tegmark, M.; Silk, J.; Rees, M. J.; Blanchard, A.; Abel, T.; Palla, F., 1997, ApJ, 474, 1T
Turk, M. J., Abel, T., & O'Shea, B. W. 2009, Science, 325, 601
Turk, M. J., Clark, P. C., Glover, S. C. O., Greif, T. H., Abel, T., Klessen, R. S., & Bromm, V., 2011, ApJ, 726
Whalen, D; Hueckstaedt, R. M.; McConkie, T. O., 2010, ApJ, 712, 101W
Wise, J. H., & Abel, T. 2008, ApJ, 685, 40
Yoshida, N., Abel, T., Hernquist, L., & Sugiyama, N., 2003, ApJ, 592, 645Y
Yoshida, N., Omukai, K., Hernquist, L., & Abel, T. 2006, ApJ, 652, 6
Yoshida, N., Omukai, K. & Hernquist, L. 2007, ApJ, 667, L117
Yoshida, N., Omukai, K., & Hernquist, L. 2008, Science, 321, 669

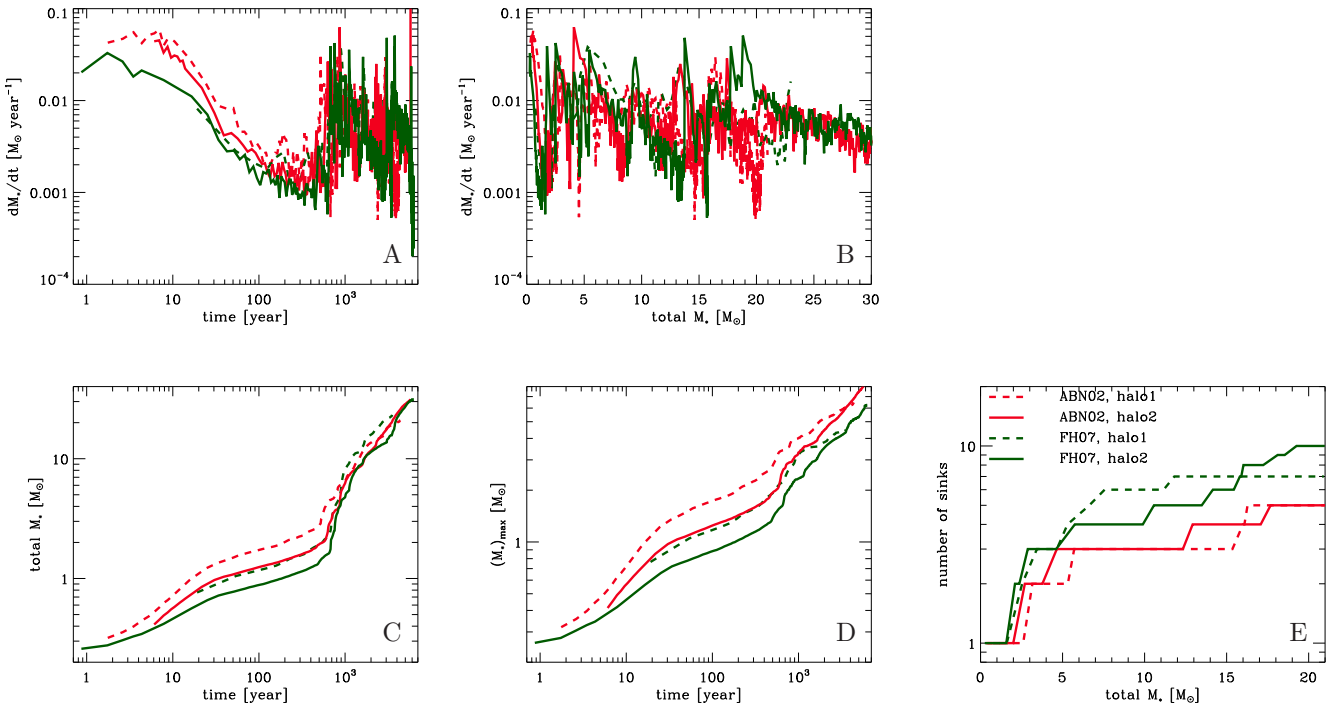

Figure 5. Time evolution of the protostellar system: Accretion rate as the function of time (A) and total mass in sink particles (B). The total mass of all the sinks particles (C) and the most massive sink particle (D) are plotted as function of time. The simulations employing FH07 produce more fragmentation than ABN02 (E).